PHYSICAL REVIEW E **77**, 066703 (2008)

# Smoothed dissipative particle dynamics model for polymer molecules in suspension

Sergey Litvinov,[1] Marco Ellero,[1,2] Xiangyu Hu,[1] and Nikolaus A. Adams[1]
[1]*Lehrstuhl für Aerodynamik, Technische Universität München, 85747 Garching, Germany*
[2]*Departamento de Física Fundamental, UNED, Apartado 60141, 28080 Madrid, Spain*
(Received 4 October 2007; published 5 June 2008)

We present a model for a polymer molecule in solution based on smoothed dissipative particle dynamics (SDPD) [Español and Revenga, Phys. Rev. E **67**, 026705 (2003)]. This method is a thermodynamically consistent version of smoothed particle hydrodynamics able to discretize the Navier-Stokes equations and, at the same time, to incorporate thermal fluctuations according to the fluctuation-dissipation theorem. Within the framework of the method developed for mesoscopic multiphase flows by Hu and Adams [J. Comput. Phys. **213**, 844 (2006)], we introduce additional finitely extendable nonlinear elastic interactions between particles that represent the beads of a polymer chain. In order to assess the accuracy of the technique, we analyze the static and dynamic conformational properties of the modeled polymer molecule in solution. Extensive tests of the method for the two-dimensional (2D) case are performed, showing good agreement with the analytical theory. Finally, the effect of confinement on the conformational properties of the polymer molecule is investigated by considering a 2D microchannel with gap $H$ varying between 1 and 10 $\mu$m, of the same order as the polymer gyration radius. Several SDPD simulations are performed for different chain lengths corresponding to $N=20-100$ beads, giving a universal behavior of the gyration radius $R_G$ and polymer stretch $X$ as functions of the channel gap when normalized properly.

DOI: 10.1103/PhysRevE.77.066703 PACS number(s): 47.11.St, 05.10.−a, 47.57.Ng

## I. INTRODUCTION

The increasing technological need to create and manipulate structures on micrometer scales and smaller for the design of micro- and nanodevices has triggered the development of many numerical methods for simulating problems at mesoscales [1–3]. One specific area of investigation is microfluidics, which refers to the fluid dynamics occurring in devices or flow configurations with the smallest design length on the order of micrometers [4]. A typical application is, for example, the dynamics of a polymer molecule in a channel or other confined geometries such as micropumps, mixers, and sensors. For instance, the mechanical response of a tethered DNA molecule to hydrodynamic flow is currently under investigation by some groups and can be used for local sensing, leading to the concept of using an immobilized DNA molecule as a mechanical-fluidic sensor or for microfabricated metallic wires and networks [5–7]. The development of single-molecule concepts is of great importance for future applications in proteomics, genomics, and biomedical diagnostics, and it is therefore evident that the ability to improve the predictive computational tools at this spatiotemporal level would greatly improve the engineering tasks.

It is worth noting that the Navier-Stokes equations describing the dynamics of a Newtonian liquid at the macroscopic level still remain valid at the microfluidic scales, therefore providing a natural framework based on the continuum description. On the other hand, it is also clear that, whenever the physical dimensions of the considered objects (i.e., polymer molecules, colloidal particles) are in the submicrometer range, the surrounding fluid starts to be affected by the presence of its underlying molecular structure, and hydrodynamic variables will be influenced by thermodynamic fluctuations according to the Landau and Lifshitz theory [8]. Standard macroscopic approaches, based, for example, on finite-volume or finite-element methods, are not suitable for this type of simulation. They neglect thermal fluctuations which, as mentioned above, are the most crucial ingredient of the mesoscopic dynamics. On the other hand, direct microscopic approaches, such as molecular dynamics, are able to resolve the smallest details of the molecular structures but they are computationally very expensive and are limited by the available computer resources. Nowadays, these approaches are restricted to computational domains of length of the order of nanometers which represent only the smallest scales (dimensions of one nanostructure) in the range covered by the considered system. Despite their high computational cost, molecular dynamics (MD) methods have been used frequently for studying the dynamics of polymer molecules in a solvent, described by Lennard-Jones interaction potentials, producing valuable results [9–11]. The advantage of these methods is that hydrodynamics emerges naturally from intermolecular interactions and does not need to be modeled.

Other methods based on Brownian dynamics techniques have been shown recently to produce accurate results for DNA dynamics in microfluidic devices [12] but require a complicated modeling of hydrodynamic interactions (in particular when coupled with the no-slip boundary conditions at the walls) mediated by a modified Rotne-Prager-Yamakawa tensor. To remedy these problems, various researchers have focused in the past on mesoscopic methods which employ numerically effective coarse-grained models retaining the relevant hydrodynamics modes. Examples are multiparticle collision dynamics [13], lattice Boltzmann methods (LBMs) [14], and dissipative particle dynamics (DPD). In particular, DPD is a mesoscopic methodology which has attracted increasing attention in recent years. DPD was originally proposed by Hoogerbrugge and Koelman in 1992 [15] and successively modified by Español and Warren in order to satisfy thermodynamic consistency [16]. The method has been shown to capture the relevant thermodynamic and hydrodynamic effects occurring in mesoscopic systems [17–20], and it has been applied in recent years to a wide range of physical situations [21–23]. Despite its great success, a number of conceptual shortcomings have been recently pointed out which affect the performance and accuracy of the technique. In particular, they concern (i) the nonarbitrary choice of the fluid equation of state, (ii) no direct connection to the transport coefficients, (iii) the unclear definition of the physical particle scales, and (iv) particle penetration due to the employed soft two-body potentials [24]. These drawbacks prevent also an *a priori* control of the spatiotemporal scale in DPD and require a tuning of model parameters in order to compare the numerical results with experimental data. All these problems can be avoided by resorting to a further improved DPD version, smoothed dissipative particle dynamics (SDPD) [25].

SDPD represents a powerful generalization of the so-called smoothed particle hydrodynamics (SPH) method [26–28] for mesoscales. Being based on a second-order discretization of the Navier-Stokes (NS) equations, transport coefficients are input parameters and do not need to be measured by Green-Kubo relations as in MD or extracted via kinetic theory as in conventional DPD. In SDPD, the particles represent therefore physical fluid elements whose specific size determines the level of thermal fluctuations in the hydrodynamic variables. At the same time, since the method is based on a Lagrangian discretization of the NS equations, hydrodynamic behavior is obtained at the particle scale and no coarse-graining assumption is needed.

In this paper, we propose a SDPD model for the investigation of the static and dynamic behavior of a polymer molecule in unbounded and confined geometries. The polymer molecule is represented by a polymer chain constituted by beads interacting by finitely extendable nonlinear elastic (FENE) forces. In order to validate the model, the two-dimensional (2D) case of a polymer molecule in a bulk solvent fluid is considered first. Note that 2D polymer dynamics does not represent an oversimplified picture of reality, but rather reflects realistic situations often encountered in polymer technology, and has recently been the focus of several numerical and experimental investigations [29–34]. In many cases polymer dynamics occurs within a very thin layer with thickness considerably smaller than the gyration radius, and the motion can be considered as truly two dimensional. Practical examples are thin polymer films, polymers adsorbed to surfaces, or polymers confined between biological interfaces. For example, recently Maier and Rädler performed experiments with a single DNA molecule electrostatically confined to a surface of fluid lipid membranes [30]. The confinement was found not to inhibit the lateral mobility of the molecule, and results for the conformational statistics were in good agreement with theoretical predictions in 2D. From a numerical point of view, extensive Monte Carlo and molecular dynamics simulations have been performed in the past and have proven to be extremely useful in corroborating analytical theories or explaining anomalous scaling behavior in bulk and confined situations [9,11,32,35].

In this work, static and dynamic scaling exponents are extracted from the SDPD simulations showing excellent agreement with the theoretical Zimm predictions and previous numerical results. As a further validation test, the case of a polymer molecule confined between two parallel walls is considered, that is, an infinite 2D microchannel. The influence that the channel gap $H$ has on the polymer conformational properties is investigated. According to previous studies in the 3D case [12,20,36], it is found that, for lengths of the gap comparable to the molecule gyration radius (i.e., on the order of micrometers), strong anisotropic effects start to affect the polymer statistics, such as, e.g., the average gyration radius and polymer stretch. In addition, the power law behavior of the polymer stretch as function of the normalized channel width has also been verified numerically, giving an exponent in excellent agreement with the analytical results predicted from scaling arguments in 2D by de Gennes [37]. The results will be discussed in the final section.

## II. THE SIMULATION METHOD

### A. Macroscopic hydrodynamics

We consider the isothermal Navier-Stokes equations on a moving Lagrangian grid

$$\frac{d\rho}{dt} = -\rho \nabla \cdot \mathbf{v}, \tag{1}$$

$$\frac{d\mathbf{v}}{dt} = \mathbf{g} - \frac{1}{\rho}\nabla p + \mathbf{F}, \tag{2}$$

where $\rho$, $\mathbf{v}$, and $\mathbf{g}$ are the material density, velocity, and body force, respectively. A simple equation of state is $p=-\kappa_T V$ where $\kappa_T$ is the isothermal compressibility. It can be rewritten as

$$p = a^2 \rho. \tag{3}$$

When Eqs. (1) and (2) are used for modeling of low-Reynolds-number incompressible flows with the artificial-compressibility method, $a$ is equal to the artificial speed of sound. An alternative equation of state for incompressible flows is

$$p = p_0\left(\frac{\rho}{\rho_0}\right)^{\gamma} + b, \tag{4}$$

where $p_0$, $\rho_0$, $\gamma$, and $a$ are parameters. The parameters in Eq. (3) and (4) may be chosen based on a scale analysis [26,38,39] so that the density variation is less than a given value. $\mathbf{F}$ denotes the viscous force

$$\mathbf{F} = \frac{1}{\rho}\nabla \cdot \Pi^{(\nu)} \tag{5}$$

where the shear stress is $\Pi^{(\nu)}=\eta(\nabla\mathbf{v}+\nabla\mathbf{v}^T)$. If the bulk viscosity is assumed as $\zeta=0$, for incompressible flow the viscous force simplifies to

$$\mathbf{F} = \nu\nabla^2\mathbf{v}, \tag{6}$$

where $\nu=\eta/\rho$ is the kinematic viscosity.

### *1. Density evolution equation*

Let us introduce the particle number density $d_i$, which is defined by

$$d_i = \sum_j W_{ij}, \tag{7}$$

where $W_{ij}=W(r_{ij},h)=W(\|\mathbf{r}_i-\mathbf{r}_j\|,h)$, and $W(r,h)$ is a generic shape function with compact support $h$ which is radially symmetric and has the properties $\int W(\mathbf{r}-\mathbf{r}')d\mathbf{r}'=1$ and $\lim_{h\to 0} W(\mathbf{r}-\mathbf{r}',h)=\delta(\mathbf{r}-\mathbf{r}')$ (in this work, a quintic spline function has been used). According to (7), $d_i$ will have larger values in a dense particle region than in a dilute particle region. Equation (7) introduces also a straightforward definition of the volume of particle $i$, which is $\mathcal{V}_i=1/d_i$. The average mass density of a particle is therefore defined as $\rho_i=m_i/\mathcal{V}_i$ where $m_i$ is the mass of a particle. Other forms of evaluating the mass density are possible in SPH, which take into account a direct discretization of the continuity equation in (1). However, the direct particle summation adopted here and based on Eq. (7) has the advantage that the total mass is algebraically conserved.

### *2. Momentum equation*

Concerning the momentum equation, it has been shown [25,40] that a possible SPH discretization of the *pressure force* appearing in (2) is

$$\frac{d\mathbf{v}_i^{(p)}}{dt} = -\frac{1}{m_i}\sum_j \left(\frac{p_i}{d_i^2}+\frac{p_j}{d_j^2}\right)\frac{\partial W}{\partial r_{ij}}\mathbf{e}_{ij}, \tag{8}$$

where $d\mathbf{v}_i^{(p)}/dt$ is the particle acceleration caused by pressure effects, $p_i$ is the pressure associated with particle $i$ [41], and $\mathbf{e}_{ij}$ is the unit vector connecting particles $i$ and $j$. It can be shown that this expression represents a second-order SPH discretization of the gradient of the scalar field $p$. Since this expression has an antisymmetric form with respect to exchange of $i$ and $j$, global conservation of momentum is satisfied. Equation (8) is similar to the form preferred by Monaghan [26].

Concerning the *viscous force*, similarly to Flekkøy *et al.* [42], the interparticle-averaged shear stress is approximated as

$$\overline{\Pi_{ij}^{(v)}} = \frac{\eta}{r_{ij}}(\mathbf{e}_{ij}\mathbf{v}_{ij}+\mathbf{v}_{ij}\mathbf{e}_{ij}) \tag{9}$$

where $\mathbf{v}_{ij}=\mathbf{v}_i-\mathbf{v}_j$. Hence, the particle acceleration due to the shear force in conservative form is given by

$$\frac{d\mathbf{v}_i^{(v)}}{dt} = \frac{\eta}{m_i}\sum_j \left(\frac{1}{d_i^2}+\frac{1}{d_j^2}\right)\frac{1}{r_{ij}}\frac{\partial W}{\partial r_{ij}}(\mathbf{e}_{ij}\cdot\mathbf{v}_{ij}\mathbf{e}_{ij}+\mathbf{v}_{ij}). \tag{10}$$

Note that this expression does not strictly conserve angular momentum. Conservation of total angular momentum can be restored by adopting either suitable artificial viscosity models based on interparticle central forces [26] for which, though, there is no direct connection to the Navier-Stokes form of the stress tensor, or linearly consistent versions of SPH [43].

## B. Mesoscopic hydrodynamics

The method outlined above is strictly analogous to the SPH technique widely used to describe macroscopic flow problems in a Lagrangian framework. In order to include mesoscopic effects, i.e., the presence of thermal fluctuations in the physical quantities, we follow the approach given by Español and Revenga, i.e., smoothed dissipative particle dynamics [25], which represents a powerful and elegant generalization of SPH at the mesoscopic scales. It should be noticed, that the method has been generalized for the study of viscoelastic liquids [44] and also, more recently, for mesoscopic multiphase flow problems [40].

### *Thermal fluctuations*

In the current SPH method the irreversible part of the particle dynamics is

$$\dot{m}_i|_{\text{irr}} = 0,$$

$$\dot{\mathbf{P}}_i|_{\text{irr}} = \eta\sum_j \left(\frac{1}{d_i^2}+\frac{1}{d_j^2}\right)\frac{1}{r_{ij}}\frac{\partial W}{\partial r_{ij}}(\mathbf{e}_{ij}\cdot\mathbf{v}_{ij}\mathbf{e}_{ij}+\mathbf{v}_{ij}). \tag{11}$$

According to the general equation for non-equilibrium reversible-irreversible coupling (GENERIC) formalism [45–47], the mass and the momentum fluctuations of particle $i$ caused by thermal noise are postulated to be

$$d\tilde{m}_i = 0,$$

$$d\tilde{\mathbf{P}}_i = \sum_j B_{ij}d\bar{\bar{\mathcal{W}}}_{ij}\cdot\mathbf{e}_{ij}, \tag{12}$$

where $d\bar{\bar{\mathcal{W}}}_{ij}$ is the traceless symmetric part of a matrix of independent increments of a Wiener process $d\mathcal{W}_{ij}=d\mathcal{W}_{ji}$, i.e., $d\bar{\bar{\mathcal{W}}}_{ij}=(d\mathcal{W}_{ij}+d\mathcal{W}_{ij}^T)/2-\text{tr}[d\mathcal{W}_{ij}]\mathbf{I}/d$, and $d$ is the spatial dimension. The isothermal deterministic irreversible equations are obtained as

$$\dot{m}_i|_{\text{irr}} = 0,$$

$$\dot{\mathbf{P}}_i|_{\text{irr}} = -\sum_j \frac{B_{ij}^2}{4k_BT}(\mathbf{e}_{ij}\cdot\mathbf{v}_{ij}\mathbf{e}_{ij}+\mathbf{v}_{ij}), \tag{13}$$

in which $k_B$ is the Boltzmann constant and $T$ is the system temperature. Comparing Eq. (13) to (11) one obtains

$$B_{ij} = \left[-4k_BT\eta\left(\frac{1}{d_i^2}+\frac{1}{d_j^2}\right)\frac{1}{r_{ij}}\frac{\partial W}{\partial r_{ij}}\right]^{1/2}. \tag{14}$$

By postulating these magnitudes for the noise terms (12), the fluctuation-dissipation theorem dictates a form for the irreversible dynamics in (13) which is exactly analogous to the SDPD discretization of the Navier-Stokes dissipation given in Eq. (10).

Note also that the kernel function $W$ needs to be a monotonically decreasing function of $r$ for $B_{ij}$ in (14) to be real valued.

In summary, the SDPD equations of motion for the fluid particles at the mesoscopic scales read

$$\frac{d\mathbf{r}_i}{dt} = \mathbf{v}_i,$$

$$\frac{d\mathbf{v}_i}{dt} = \frac{d\mathbf{v}_i^{(p)}}{dt} + \frac{d\mathbf{v}_i^{(v)}}{dt} + \frac{1}{m_i} d\tilde{\mathbf{P}}_i, \tag{15}$$

with $d\mathbf{v}_i^{(p)}/dt$, $d\mathbf{v}_i^{(v)}/dt$, and $d\tilde{\mathbf{P}}_i$ being given, respectively, in Eqs. (8), (10), and (12).

### C. Solid wall modeling

In this work, we consider periodic boundary conditions to model a bulk fluid and solid boundary conditions for confined situations. In the latter case, the solid body region is filled with virtual particles [48]. Whenever the support of a fluid particle overlaps with the wall surface, a virtual particle is placed inside the solid body, mirrored at the surface. The virtual particles have the same volume (i.e., mass and density), pressure, and viscosity as their fluid counterparts but the velocity is given as $\mathbf{v}_{\text{virtual}} = 2\mathbf{v}_{\text{wall}} - \mathbf{v}_{\text{real}}$ for a no-slip velocity boundary condition or $\mathbf{v}_{\text{virtual}} = \mathbf{v}_{\text{real}}$ for a free-slip boundary condition. Currently, only straight channel walls are considered. For curved wall surfaces, the virtual particle approach may introduce considerable errors. To increase the accuracy near curved surfaces, Takeda *et al.*[49], Morris *et al.*[38], and more recently Ellero *et al.* [50] have introduced special wall particles which interact with the fluid particles in such a way that more general boundary conditions are represented accurately.

### D. Mechanical modeling of the polymer chain

The model for the polymer molecule in suspension adopted in this work can be described in the following terms. The solvent liquid is represented by SDPD particles which represent physical elements of fluid containing potentially thousands of solvent (i.e., water) molecules and interacting hydrodynamically. Concerning the polymer model, we consider it as a linear chain of polymer beads, each bead being represented as a mixture of real polymer monomers together with solvent molecules. The numerical realization of this physical model is obtained by selecting a number of SDPD fluid particles and letting them interact, as well as hydrodynamically, also by additional finitely extendable nonlinear elastic springs

$$\mathbf{F}^{\text{FENE}}(\mathbf{r}_{ij}) = \frac{K\mathbf{r}_{ij}}{1 - (r/R_0)^2}, \tag{16}$$

where $K$ is the spring constant, $r = \sqrt{\text{tr}(\mathbf{r}_{ij}\mathbf{r}_{ij})}$ is the bead-bead distance, and $R_0$ represents the maximum extensibility.

A typical configuration is sketched in Fig. 1. Light-blue particles represent the fluid while dark-blue particles are the beads forming the model polymer chain. All particles interact by the hydrodynamics forces given in Eq. (15). Polymer beads interact with each other additionally by the FENE forces which produce an elastic contribution due to the portion of real polymer monomers assumed to be contained in the bead.

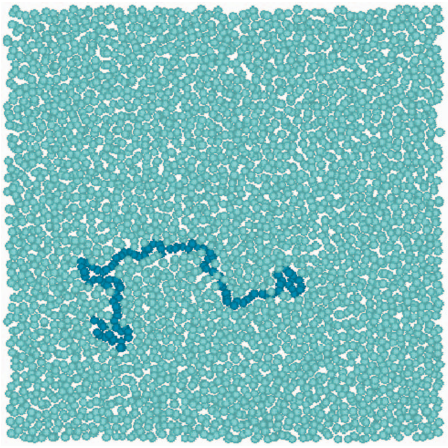

FIG. 1. (Color) Typical simulation configuration: light-blue particles represent solvent particles and dark-blue particles represent polymer beads. All particles interact by the hydrodynamic forces given in Eq. (15). Beads interact with each other additionally by FENE forces. In order to simulate bulk conditions, standard periodic boundary conditions are employed at the edges of the simulation box. For this case a total number of $N_p = 3600$ particles were considered. Among them, $N = 100$ particles were selected as beads defining the polymer chain.

According to the previous discussion, hydrodynamic interactions between polymer beads occur via *viscous* and *pressure* terms and are justified by the fact that within every bead there is a large amount of water molecules which produce hydrodynamic behavior on the same scale as the SDPD particle.

Note that excluded-volume effects are directly taken into account through the pressure terms appearing in the discretized hydrodynamic equations (8) which produce repulsive forces between approaching particles, and therefore there is no need to introduce short-range Lennard-Jones forces between beads. It should be noted also that, by considering a bead as a special case of a SDPD particle, we bypass the problem of modeling separately the *hydrodynamic coupling* of polymer beads and solvent particles which is taken into account through the SDPD friction forces in Eq. (10). Since these forces are written in antisymmetric form with respect to the particle indices, they conserve exactly the total linear momentum also during fluid-bead interactions. This represents a remarkable advantage compared to LB methods, where special models must be introduced for the fluid-bead interactions in order to conserve the total linear momentum of the system [14].

In summary, the momentum equation for the bead $i$ reads

$$m_i \frac{d\mathbf{v}_i}{dt} = \mathbf{F}_i^{\text{hydro}} + \mathbf{F}_{i,i_1}^{\text{FENE}} + \mathbf{F}_{i,i_2}^{\text{FENE}}, \tag{17}$$

$\mathbf{F}_i^{\text{hydro}}$ being the total sum of the resulting SDPD forces acting on particle $i$ given in Eq. (15), and $i_1, i_2$ the two next neighboring beads of bead $i$ in the polymer chain.

A final remark on the structure of these equations is in order. As can be seen in Eq. (16), the additional bead-bead interaction, although entropic in origin, appears as a consequence of the GENERIC framework in the model Eq. (17) as an ordinary interparticle force [51]. Therefore, there is no particular concern about the general structure of the modified SDPD model equations which is still consistent with the GENERIC model. In particular, the magnitudes of the stochastic terms are uniquely prescribed in terms of the dissipative forces between the particles, which in this model remain unaltered.

## III. NUMERICAL SETUP

In this work, the statistical properties of a single polymer molecule immersed in a Newtonian liquid under good solvent conditions are investigated in an infinite domain and in a confined geometry. In the first case, the simulation domain is represented by a 2D square box of physical length $L=10^{-5}$ m. A total number $N_p=3600$ of SDPD particles is used. Among them, $N$ particles representing polymer beads are selected and allowed to interact by the FENE forces. $N$ ranges from 20 to 100. Concerning the input parameters entering the FENE model, we choose $K=5.3$ N m$^{-1}$ and $R_0=4\Delta r$, where $\Delta r=1.66\times 10^{-7}$ m is the initial particle spacing [52].

Fluid particles interact by the forces given in Eq. (15) with cutoff radius $h=5.0\times 10^{-7}$ m, and the kernel function used is a quintic spline kernel. This implies an average number of 20 neighboring SDPD particles entering the interpolation process.

Depending on the particular case, periodic or solid boundary conditions are used. In the latter case, solid walls are modeled by virtual particles as discussed in Sec. II. The method prevents particles penetrating the solid wall (impermeability condition) and forces the tangential component of the fluid velocity to be exactly zero at the interface (no-slip condition) [40]. The previous conditions are crucial in taking into account hydrodynamic effects due to the confinement.

Concerning the solvent, we consider a Newtonian fluid characterized by a dynamic viscosity $\mu=10^{-6}$ kg m$^{-1}$ s$^{-1}$ and $\rho=10^3$ kg m$^{-3}$, and the fluid temperature is set to $T=300$ K. According to these parameters, the solvent is ideally good and $\theta$ collapse never occurs. Concerning the numerical integration of the equations of motion for the particles, a second-order predictor-corrector scheme is used. To maintain numerical stability, a Courant-Friedrichs-Lewy time step restriction based upon artificial sound speed (isothermal compressibility), body force, and viscous dissipation [38,53,54] is employed. When thermal fluctuations are introduced in the mesoscopic simulation, the time steps are further decreased to recover the correct kinetic temperature. The artificial speed of sound of the solvent liquid keeps relative density fluctuations below 1% and models a quasi-incompressible fluid.

Statistical averages are computed by extracting independent polymer configurations. The production run is performed after an equilibration period (500–2000 time steps depending on the length of the polymer chain) in order to avoid spurious effects due to the initial nonrandom polymer configuration.

Finally, a remark on the numerical efficiency of the method is in order. The operation count of SDPD, as for DPD or any other particle method, scales as $N_p \log N_p$ when proper linked-list cell algorithms are employed. However, the fact that the mass density $\rho_i$ must be evaluated for every particle before calculating the interaction forces makes it potentially slightly slower. Nevertheless, the conceptual and technical advantages gained from the thermodynamical consistency of SDPD and its direct connection to the Navier-Stokes equations overwhelm the performance penalty.

## IV. SIMULATION RESULTS

In this section, the conformational properties of the polymer molecule are investigated in a two-dimensional space. The objective is twofold: First, we apply the SDPD method to the study of a polymer molecule in an infinite solvent medium under zero-flow condition. In this case, the stochastic Wiener process entering Eq. (15) represents the only forcing term mimicking the presence of thermal fluctuations in the system. Under these conditions, the flow is isotropic, and theoretically predicted universal scaling laws for several polymer properties can be tested numerically. In particular, the static and dynamic behavior of the conformational polymer properties as well as the structure factor have been intensely studied using a variety of methods [9,10,14] and are compared here with the present results.

Second, the effect of geometrical confinement, in particular due to the presence of solid walls in microchannels, is investigated. This is an important validation test because it allows us to estimate the accuracy of SDPD in simulating real geometries encountered in microfluidic devices. It is generally known that confinement alters dramatically the behavior of a polymer molecule which in a microchannel, for example, will extend along the channel axis to a substantial fraction of its contour length. Scaling laws for the dependence of the polymer stretch upon the channel width have been proposed theoretically [37] and validated numerically in a number of 3D situations. As a further test for the SDPD method, the two-dimensional static properties of a polymer molecule confined in a microchannel are investigated and the results are compared with previous theoretical and numerical work [12,20,36].

### A. Conformational properties of a polymer in a bulk medium

#### *1. Chain statics*

Conformational properties of a polymer chain, in particular deformation and orientation, can be analyzed by monitoring the evolution of several tensorial quantities such as, for instance the *gyration tensor*

$$\mathbf{G} \equiv \frac{1}{2N^2}\sum_{i,j}\langle \mathbf{r}_{ij}\mathbf{r}_{ij}\rangle, \tag{18}$$

or the *end-to-end tensor* defined as

$$\mathbf{R} \equiv \langle (\mathbf{r}_N - \mathbf{r}_1)(\mathbf{r}_N - \mathbf{r}_1)\rangle. \tag{19}$$

Here, $\mathbf{r}_{ij}=\mathbf{r}_j-\mathbf{r}_i$ with $\mathbf{r}_i$ being the position of the $i$th bead in the chain. The indices $i,j$ run from 1 to $N$, the total number of beads. Related quantities are the *radius of gyration* $R_G$

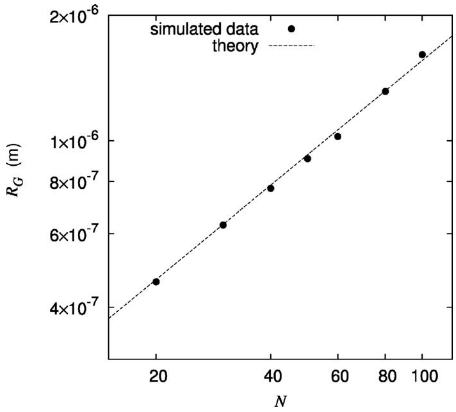

FIG. 2. Scaling of the radius of gyration $R_G$ for several chain lengths corresponding to $N=20,30,40,50,60,80,100$ beads. The dotted line represents the best fit consistent with the theory ($R_G \propto N^{\nu}$) and gives a static exponent $\nu=0.76\pm0.012$.

$=\sqrt{\mathrm{tr}\,\mathbf{G}}$ and the *end-to-end radius* $R_E=\sqrt{\mathrm{tr}\,\mathbf{R}}$. The effect of the number of beads $N$ on $R_G$ and $R_E$ is known to follow the analytical expressions

$$R_E = a_E(N-1)^{\nu},$$

$$R_G = a_G[(N^2-1)/N]^{\nu}, \tag{20}$$

where $\nu$ is called the *static factor exponent* and, from renormalization theory, it assumes the value $\nu\approx0.588$ in three dimensions, with $a_E$ and $a_G$ being suitable constants. In the limiting case of $N\gg1$, both quantities scale as $R_E\approx R_G\propto N^{\nu}$. Notice that this result is valid only in three dimensions. Because the goal of this work is to test the numerical scheme first in a 2D case, the static exponent $\nu$ extracted by our simulations should be compared with the analogous two-dimensional Flory formula, which gives a value 0.75 in good solvent conditions [37,55]. This value has been verified recently by several authors using molecular dynamics simulations [32–34].

In order to extract the exponent $\nu$, SDPD simulations have been carried out with five different chain lengths characterized by $N=20,40,60,80,100$ beads. In all cases the time-averaged values of the gyration radius $R_G$ have been evaluated from several independent steady-state polymer configurations. Figure 2 shows a log-log plot of the time-averaged $R_G$ versus $N$. Error bars are within the symbol dimensions. The results can be fitted (dotted line in the figure) by a power law with exponent $\nu=0.76\pm0.012$, which is in good agreement with theoretical results and previous numerical investigations. It should be noticed that this way to evaluate $\nu$ is quite time consuming since simulations at large $N$ are necessary in order to fit accurately the data in Fig. 2.

An alternative way to extract $\nu$ is, instead of using the scaling law (20), by employing the static structure factor defined as

$$S(\mathbf{k}) \equiv \frac{1}{N}\sum_{i,j}\langle \exp(-i\mathbf{k}\cdot\mathbf{r}_{ij})\rangle. \tag{21}$$

In the limit of small wave vector $|\mathbf{k}|R_G\ll1$, the structure factor can be approximated by $S(\mathbf{k})\approx N(1-\mathbf{k}^2R_G/3)$, while for $|\mathbf{k}|R_G\gg1$ $S(\mathbf{k})\approx 2N/\mathbf{k}^2R_G$ holds. The intermediate regime $|\mathbf{k}|R_G\sim1$ contains information about the intramolecular spatial correlations. In the absence of external perturbation and close to equilibrium, $S(\mathbf{k})$ is isotropic and therefore depends only on the magnitude of the wave vector $k=|\mathbf{k}|$. $S(k)$ probes therefore different length scales even for a single polymer, and in the intermediate regime is shown to behave like

$$S(k)\propto k^{-1/\nu}. \tag{22}$$

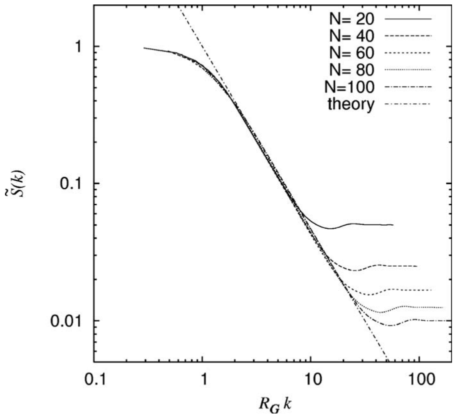

FIG. 3. Normalized equilibrium static structure factor $\tilde{S}(k)=S(k)/S(0)$ versus $R_Gk$ corresponding to several chain lengths. All the curves collapse on a master line for $2<R_Gk<8$ (scaling regime). In this region $\tilde{S}(k)\propto k^{-1/\nu}$ with $\nu=0.75$ (dotted line).

Figure 3 shows a log-log plot of $S(k)$ vs $R_Gk$. From this figure it is possible to see how curves evaluated from simulations with different chain lengths ($N$) collapse on a single curve for $2<R_Gk<8$, the slope of the linear region being $-1/\nu$. The dotted line in the figure represents the theory with $\nu=0.75$ and shows very good agreement with the SDPD results.

This way provides a more efficient route to calculate the static exponent $\nu$, since one single simulation with $N=20$ is sufficient for accurate estimates.

These two tests are commonly performed to validate the equilibrium conformational properties of a FENE polymer molecule. These scaling laws have been also verified by other techniques such as, for instance, DPD in three dimensions [17].

### *2. Chain dynamics*

The dynamic conformational behavior of the polymer molecule represents another important feature that must be checked. The starting point is the *dynamical structure factor* defined as

$$S(\mathbf{k},t) \equiv \frac{1}{N}\sum_{i,j}\langle \exp\{-i\mathbf{k}\cdot[\mathbf{r}_i(t)-\mathbf{r}_j(0)]\}\rangle. \tag{23}$$

Dynamic scaling arguments applied to the Zimm model in isotropic conditions predict a functional form of $S(k,t)$ of the type

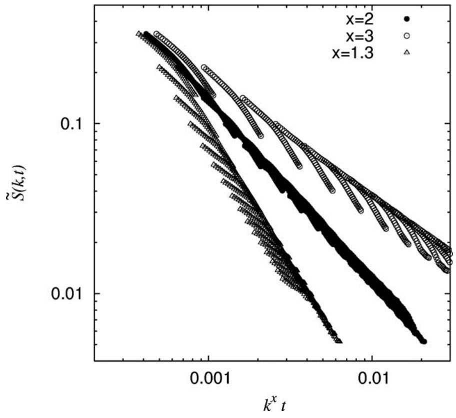

FIG. 4. Scaling plot of the normalized dynamic structure factor $\tilde{S}(k,t)=S(k,t)/S(k,0)$ for $N=20$ in log-log coordinates. The best collapse for $x=2$ is clearly visible. For different dynamic exponents $(x=1.3,3)$, the 2D data fail to collapse on a single curve. The range of $k$ was consistent with the scaling regime $2<R_G k<8$.

$$S(k,t)=N(kR_G)^{(-1/\nu)}F[tD_G R_G^{-2}(kR_G)^x] \tag{24}$$

where $x=2+\nu_D/\nu$ (dynamical scaling exponent), $D_G$ is the diffusion constant, and $\nu_D$ is the diffusion scaling exponent. Therefore, if we plot $S(k,t)/S(k,0)$ vs $tk^x$, in the scaling regime, a universal curve should be obtained for all the values of $k$ and $t$. This is indeed predicted by the theory with a scaling exponent $x=3$ in 3D. Although the result has been verified in the three-dimensional case, anomalous scaling has been observed in the two-dimensional case, giving a value $x=2$. The goal here is to verify this result with the present SDPD model.

Figure 4 shows the dynamical structure factor data plotted versus $k^x t$ for three different values of the dynamic scaling exponent, that is, $x=1.3,2,3$. The figure suggests that in the appropriate scaling regime (that is, $2<R_G k<8$ from Fig. 2) the best collapse is obtained indeed for $x=2$ whereas, for $x=1.3$ and 3, the data indeed do not exhibit any collapse. This confirms the previous results indicating that anomalous scaling occurs in 2D polymer dynamics [32]. It should be noticed that, if we assume $D_G \propto N^{-\nu_D}$, this result implies that $\nu_D=0$ for the chain diffusion constant in 2D. Indeed, this has been recently verified given the logarithmic scaling of $D_G$ with $N$ [33,34].

### *3. Rouse mode analysis*

As a further test of the polymer dynamics we calculate the internal modes of the chain. This can be done by evaluating the so-called Rouse coordinates $\mathbf{R}_p$ defined as

$$\mathbf{R}_p=\frac{1}{N}\sum_{n=1}^{N}\cos\left(\frac{p\pi\left(n-\frac{1}{2}\right)}{N}\right)\mathbf{r}_n, \tag{25}$$

where $\mathbf{r}_n$ is the position of the bead $n$ and $p=0,1,2,\ldots,N$ are the normal modes of a polymer chain constituted of $N$ beads. For example, $\mathbf{R}_0$ is the chain's center of mass, while $\mathbf{R}_p$ for $p>1$ represent high-order modes describing the internal motion of the polymer molecule.

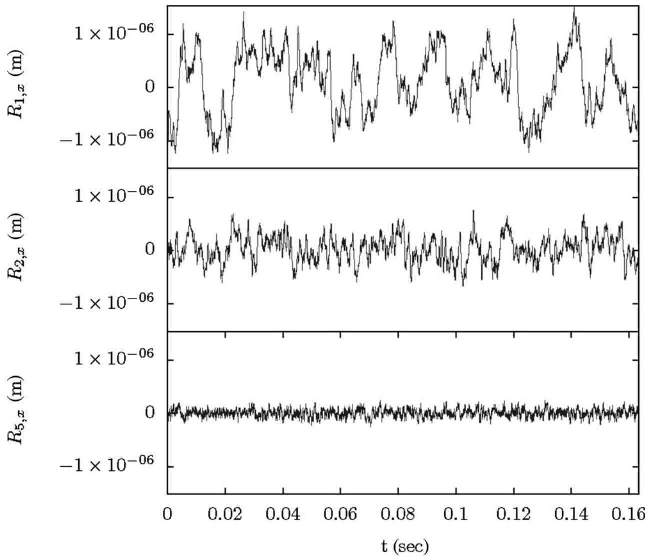

FIG. 5. Rouse coordinate histories for $R_{p,x}$ with $p=1,2,5$ and a chain length $N=80$. The magnitudes of fluctuations decrease with increasing $p$ according to analytical theories.

In Fig. 5 the Rouse coordinate histories for the $x$ direction are plotted for three different modes $p=1,2,5$ corresponding to a polymer chain with $N=80$ beads. Analogously to what was observed in [11], all these quantities fluctuate around zero with magnitudes decreasing for increasing values of $p$. In order to quantify the level of fluctuations we define the mean square Rouse coordinate as

$$\langle \mathbf{R}_p^2\rangle=\frac{1}{2N^2}\sum_{n,m=1}^{N}\cos\left(\frac{p\pi\left(n-\frac{1}{2}\right)}{N}\right)\cos\left(\frac{p\pi\left(m-\frac{1}{2}\right)}{N}\right)\times\langle(\mathbf{r}_n-\mathbf{r}_m)^2\rangle. \tag{26}$$

It has been recently shown that, for long chains, this quantity scales as $\sim p^{-(2\nu+1)}$, where $\nu$ is the static scaling exponent [11]. For the two-dimensional case, a scaling exponent $(2\nu+1)\approx 5/2$ should be observed. Figure 6 shows the mean square amplitude $\langle \mathbf{R}_p^2\rangle$ for different chain lengths $(N=20,40,60,80,115)$ versus the mode index $p$. The picture confirms the observation of Fig. 5 showing a monotonic decrease of $\langle \mathbf{R}_p^2\rangle$ vs $p$. The solid line represents the best fit which, for $N=115$, gives a value of the slope equal to $-2.61\pm0.05$ in reasonable agreement with the value $-2.5$ predicted by the theory for the two-dimensional case. This value was calculated by using the static scaling exponent $\nu=0.75$ obtained from the results in the previous section. In addition, an increasing trend of $\langle \mathbf{R}_p^2\rangle$ vs $N$ is also observed in Fig. 6 in agreement with the analytical results, which predict a dependence $\sim N^{2\nu}$ [11].

### *4. Diffusion coefficient*

In this section we present results for the center-of-mass (c.m.) diffusion coefficient $D$ of the polymer molecule. This is evaluated from the mean square displacement of the center of mass defined as

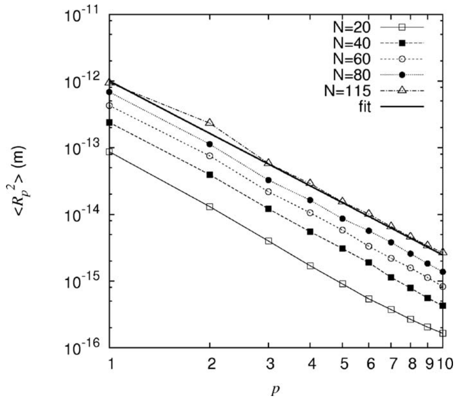

FIG. 6. Rouse mode mean square amplitudes $\langle R_p^2 \rangle$ vs mode $p$ for different polymer chains corresponding to $N=20,40,60,80,115$ beads. The decrease of fluctuations with increasing value of $p$ is clear. The solid curve represents the best fit of the data corresponding to $N=115$ and gives a slope equal to $-2.61 \pm 0.05$, in good agreement with the theory.

$$[\Delta \mathbf{R}_0(t)]^2 = \langle [\mathbf{R}_0(t+t_0) - \mathbf{R}_0(t_0)]^2 \rangle \tag{27}$$

where $\mathbf{R}_0$ is defined by (25). The single-chain diffusion coefficient is finally computed from the equation

$$[\Delta \mathbf{R}_0(t)]^2 = 4Dt \tag{28}$$

in the limit of large $t$, when the linear regime is reached.

Previous studies in the three-dimensional case indicate that strong box-size effects in the evaluation of $D$ occur. These finite-size corrections are of the order of $1/L$; hence, in principle, it is easy to determine the diffusion coefficient in the thermodynamic limit ($L \to \infty$) by simply plotting $D$ versus $1/L$ and extrapolating the value at the intercept of the $y$ coordinate [18]. These results have been shown to produce a scaling relation, that is, $D_\infty(N)$ collapses on a master curve proportional to $N^{-\nu_D}$, $\nu_D=0.59$ being the dynamic scaling exponent.

The situation is more subtle in two dimensions due to the infinite range of the hydrodynamic interactions. Consistency with our evaluation of the dynamic scaling factor ($x=0$) would require $\nu_D=0$. In order to verify it, we plotted the data for $D$ vs $N$ logarithmically for different values of $L$ and $N$, namely, $N=10,20,40$ and $L=0.75\times10^{-5}, 1.0\times10^{-5}, 1.25\times10^{-5}$, and no collapse was found. However, a decreasing scaling exponent (slope of the curves) was observed as the system size increased, analogously to previous findings [18]. In order to check quantitatively that $\nu_D=0$, Falck *et al.* [33]. proposed an analytical formula for the 2D diffusion coefficient of a polymer molecule which reads

$$D = \frac{k_B T}{2\pi\mu}[-\ln(R_g/L) + \text{const} + O((R_g/L)^2)]. \tag{29}$$

Note that this expression explains also why it is impossible to extrapolate $D$ in the thermodynamic limit, obtaining for $L \to \infty$ divergent values.

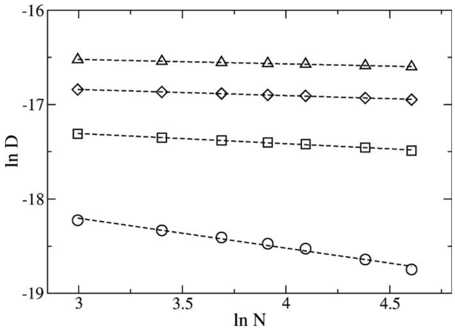

FIG. 7. Dependence of the diffusion coefficient $D$ on $N$ for different cutoff lengths $L_{\text{cut}}$ in Eq. (29): (○) $L_{\text{cut}}=10^{-5}$ m, (□) $L_{\text{cut}}=10^{-3}$ m, (◇) $L_{\text{cut}}=10^{-1}$ m, and (△) $L_{\text{cut}}=10$ m.

Following Falck *et al.* [33], in order to check the behavior of $D$ vs $N$ in the limit of large box sizes, we have inserted the values of the gyration radii $R_g$ evaluated in Sec. IV into Eq. (29) and evaluated the curves for several numbers of beads $N \in [20:100]$ and for several cutoff lengths $L=L_{\text{cut}} \in [1.0\times10^{-5}:10]$ m. Note that, because the thermodynamic limit is not defined, we select arbitrarily large but finite values $L_{\text{cut}}$ in Eq. (29) and look at the trending behavior of $D(N)$. The results are shown in Fig. 7: as reported in [33], the slopes of the curves ($\nu_D$) decrease monotonically from 0.32 (smallest cutoff) to 0.04 (largest cutoff), according with $x=0$ previously evaluated.

### B. Effect of confinement on the polymer conformation

As already mentioned, confinement between two parallel walls significantly affects the polymer configuration statistics and induces anisotropic effects. The situation is the following. A polymer molecule is immersed in a Newtonian solvent modeled with SDPD particles. Periodic boundary conditions are applied at the edges of the box in the $x$ direction while solid boundary conditions using virtual particles are applied at the top and at the bottom of the simulation box thereby confining the solvent between two impenetrable walls placed a distance $H$ apart (channel width).

Kong *et al.* in 1994 [20] performed DPD simulations of this system and analyzed the components of the polymer gyration radius parallel and perpendicular to the confining walls. The results were clearly indicating anisotropic statistics and showed the collapse of the results for different chain lengths on a universal curve as a function of the normalized channel width.

The objective here is to validate our numerical model in the two-dimensional case analogous to that described above. The first issue is to show that a similar universal scaling can be obtained for different chain lengths and channel widths. We performed simulations with polymer molecules modeled with $N=20,60$ beads and channel gaps $H$ ranging from 1 to 10 $\mu$m. The length of the box in the periodic direction was chosen such that $L_x > 4R_G$. This choice ensures that statistical averages are independent of the box size in the periodic direction [36].

In order to observe an anisotropic effect it is convenient to decompose the gyration radius $R_G$ into components parallel and perpendicular to the walls as follows:

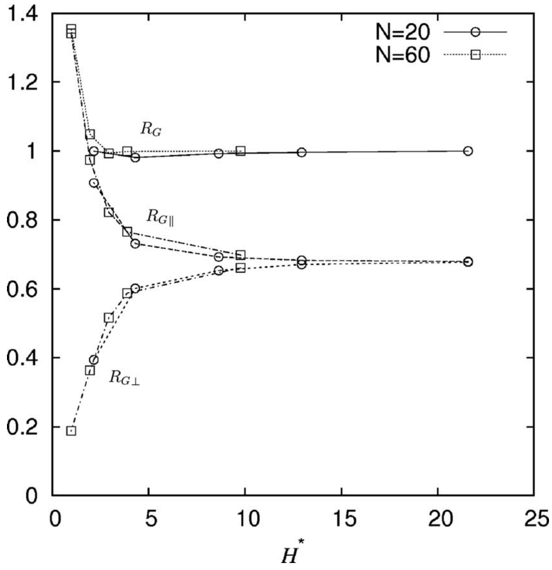

FIG. 8. Variation of the normalized gyration radius $R_G^*$ together with its parallel ($R_{G\parallel}^*$) and perpendicular ($R_{G\perp}^*$) components. The data correspond to different chain lengths ($N=20,60$) and values of the normalized channel gap $H^*$ ranging from 1 to 22. All the quantities have been made dimensionless by the gyration radius $R_G^\infty$ of the corresponding polymer molecule without confinement.

$$R_{G\parallel} = \frac{1}{2N^2}\sum_{i,j}\langle x_{ij}^2\rangle, \quad R_{G\perp} = \frac{1}{2N^2}\sum_{i,j}\langle y_{ij}^2\rangle, \tag{30}$$

where $x_{ij}=x_i-x_j$ and $y_{ij}=y_i-y_j$. Figure 8 shows these components together with the gyration radius $R_G$ plotted for different values of the channel gap $H$. All the quantities have been made dimensionless by dividing them by the relative bulk free radii of gyration $R_G^\infty$ corresponding to the respective chain length and given in Fig. 2; for example, $H^*=H/R_G^\infty$. The excellent collapse of the results for different chain lengths on a single curve indicates that universal scaling is obtained, analogously to previous works [36]. For large ratios $H^*$, the results are consistent with the bulk behavior and no anisotropies are observed. For values of $H^*$ smaller than 14, slight departures in the results are visible, which become evident for $H^*<10$, where $R_{G\parallel}^*$ starts to differ remarkably from $R_{G\perp}^*$. For decreasing values of $H^*$, $R_{G\perp}^*$ tends to zero while $R_{G\parallel}^*$ continues to increase toward larger values: for $H^*=1$, $R_{G\parallel}^*\approx 1.35$.

Unlike previous DPD simulations [20,36], in this work $R_{G\parallel}^*$ is found to be strongly dependent on the confinement, which supports the common perception that the average polymer molecule orientation becomes increasingly aligned with the channel axis depending on the gap $H^*$. Diverging values of the parallel and perpendicular components of the gyration radius for a polymer molecule confined in a slit and in a cylinder have been documented by Cifra *et al.* [56] in qualitative agreement with our findings.

Another interesting feature is represented by the dependence of the global gyration radius $R_G^*$ on the channel gap. Indeed, although deviations in $R_{G\parallel}^*$ and $R_{G\perp}^*$ start to be visible already for $H^*\approx 10$, $R_G^*$ remains nearly constant up to $H^*\approx 3$. For $H^*<3$, a sudden increase takes place due to the diverging values assumed by $R_{G\parallel}^*$.

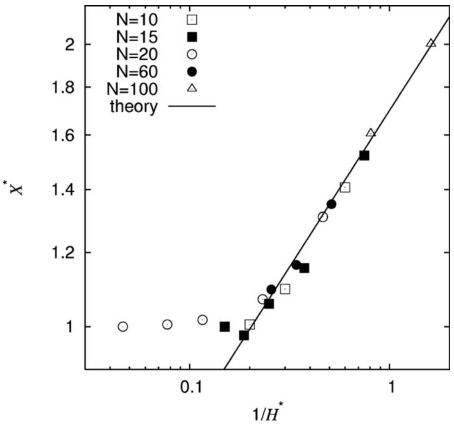

FIG. 9. Normalized polymer stretch $X^*$ as a function of the inverse of the channel gap $H^*$ for several chain lengths ($N=10,15,20,60,100$). Deviations from the bulk behavior appear at $1/H^*\approx 0.2$. For $1/H^*>0.4$ universal scaling is realized, the slope of the fitted line being $z=1/3$ (theory).

If we describe the conformational state of the polymer molecule in terms of an ellipsoid, then it is clear from Fig. 8 that different regimes can be observed. In almost unconfined conditions ($H^*>12$), the principal axes of the ellipsoid are randomly distributed in space and this is reflected by the equal values assumed by $R_{G\parallel}^*$ and $R_{G\perp}^*$; the presence of solid walls has no effect in this situation. A second regime can be characterized for values of the channel gap $3<H^*<12$ (slight confinement) where the ellipsoid tends to align itself on the channel axis preserving, however, its overall statistical length. In this regime, $R_G^*$ remains constant and the polymer molecule does not undergo any net deformation. Finally, the sudden increase of $R_G^*$ for $H^*<3$ (strong confinement) reflects the overall stretching of the polymer chain induced by the presence of the parallel walls which try to squeeze it along the channel axis.

In [56] a similar behavior was reported; in that work Cifra noticed also the presence of a minimum in $R_G^*$ located at $H^*\approx 2$, before the sharp increase happens. This is only slightly visible in Fig. 8 where $R_G^*$ exhibits a smaller value compared to the bulk for $H^*\approx 3$ (see the third squared symbol from the left). Statistical errors in the results, however, do not allow for further comparisons. Longer simulations as well as more extensive parameter studies of $H^*$ in this region would be necessary to confirm the analogy.

In order to compare these results quantitatively, we plotted in Fig. 9 the polymer stretch $X$ as a function of the channel gap $H$. Instantaneous polymer stretch represents the maximum extension of the molecule along the channel direction and it is defined as

$$X(t) = \max_{i=1,\ldots,N}[x_i(t)] - \min_{i=1,\ldots,N}[x_i(t)]. \tag{31}$$

In Fig. 9, the corresponding dimensionless quantities $X^*=X/X^\infty$ and $H^*=H/R_G^\infty$ are plotted, $X^\infty$ being the equilibrium polymer stretch in an unconfined domain and $X=\langle X(t)\rangle$. Ana-

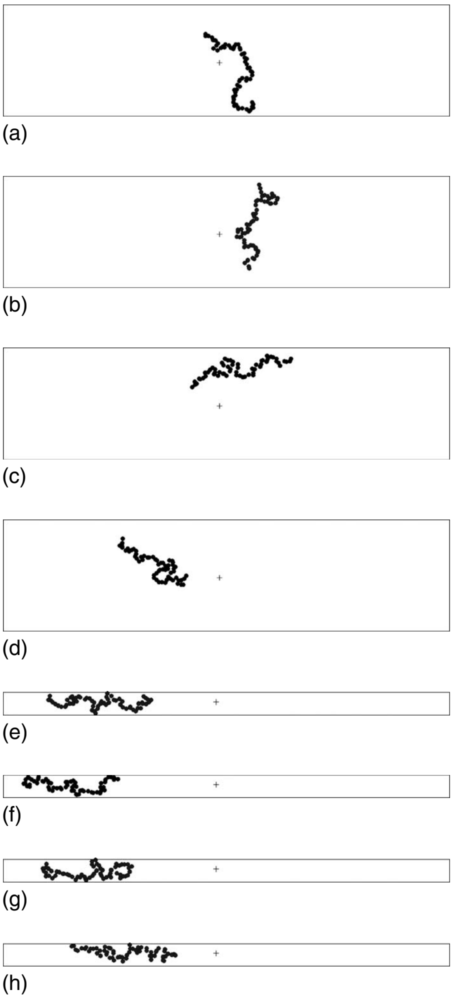

FIG. 10. Polymer conformations taken respectively after 1000, 2000, 4000, and 6000 time steps ($N=60$ beads). The free gyration radius for this chain is $R_G^\infty=1.02$ $\mu$m while the channel gap is $H=5.0$ (four top figures) and 1.0 $\mu$m (four bottom figures). The corresponding ratio is $H^*\approx 5$ and 1, respectively.

lytical theories predict scaling behavior and give $X^* \propto (H^*)^{(-2/3)}$ in a 3D square channel of width $H^*$. Recently, these results have been validated numerically by Jendrejack *et al.* using Brownian dynamics techniques [12], showing a good agreement with the de Gennes theory in 3D. Figure 9 shows the analogous scenario in a two-dimensional case for different chain lengths $N=10,15,20,60,100$. Excellent scaling behavior is obtained. Similarly to what is observed in [12], $X^*$ remains constant up to values of $1/H^*$ approximately equal to 0.2 where confinement effects start to be visible, while for $1/H^*>0.4$ the scaling regime is fully realized. The slope of the approximate fitted curve prescribes a scaling law $H^{*(-z)}$ where $z=1/3$ in good agreement with the the Gennes theory in two dimensions. Notice that the previous result differs from the 3D case studied by Jendrejack *et al.* [57] where the scaling exponent takes a value equal to 2/3.

Finally, Fig. 10 shows several time snapshots (after 1000, 2000, 4000, and 6000 time steps) of the polymer configuration for two different channel widths: $H=5.0$ (four snapshots from the top) and 1.0 $\mu$m (four snapshots from the bottom). The polymer chain consists of $N=60$ beads and its free gyration radius is $R_G^\infty=1.02$ $\mu$m, therefore providing values of the ratio $H^*$ approximately equal to 5 and 1. From the first four snapshots, it is possible to see qualitatively also that a channel gap of 5.0 $\mu$m will not affect strongly the polymer statistics. The polymer molecule is free to rotate in the channel similarly to the bulk case. This situation is indeed reflected in Figs. 8 and 9 which show quantitatively that the averaged gyration radius and polymer stretch are not affected in this regime and anisotropies in the gyration radius components are small. However, for smaller channel gaps $H$, the polymer conformations exhibit a totally different behavior (Fig. 10, bottom). For $H=1.0$ $\mu$m it is evident that the polymer maintains its average orientation at any time; therefore confinement has its main effect in inhibiting angular movements of the polymer in the direction perpendicular to the walls. The observed enhanced alignment of the polymer chain for this channel width must necessarily have a big impact on the statistics. This observation is confirmed by inspection of Fig. 8 which shows that $R_{G\parallel}^*$ is more than six times larger than $R_{G\perp}^*$.

## V. FINAL REMARKS, OUTLOOK, AND CONCLUSIONS

In this study, a smoothed dissipative particle dynamics method for mesoscopic flows has been formulated for a polymer molecule suspended in a Newtonian liquid. The SDPD model represents a generalization of smoothed particle hydrodynamics to the mesoscale which is thermodynamically consistent, i.e., it respects the first and second laws of thermodynamics and introduces thermal fluctuations according to the fluctuation-dissipation theorem. Although the starting point is represented by a particle discretization of the macroscopic hydrodynamics (SPH), the method can be also interpreted as an improved version of DPD, where the original repulsive and friction forces acting between DPD particles are tightly connected to second-order discretizations of pressure and viscous terms present in the Navier-Stokes equations.

The method is used to study the configurational behavior of the polymer chain in bulk and confined geometries. In the unbounded case, exact static and dynamic scaling relations have been found according to the Zimm theory in two dimensions. In the context of microfluidics, the effect of confined geometries on the conformational properties of the polymer molecules has been analyzed showing results in agreement with previous numerical experiments. The results suggest that the method can be faithfully applied to mesoscopic flow problems at microscales where the effect of hydrodynamic interactions as well as microconfinement play a central role. In the present study, the model is validated for two-dimensional test cases. Extension of the algorithm to the three-dimensional case and its parallel implementation are currently under work. This should allow one to handle in the near future full-scale problems encountered in realistic microfluidics applications such as the micromechanical behavior of DNA molecules under different hydrodynamic flow conditions [5–7].

A final discussion on the Schmidt number is in order. The Schmidt number is defined as $\mathrm{Sc}=\nu/D$, where $\nu$ is the kinematic viscosity of the solvent and $D$ the molecular diffusivity. Strictly speaking, the applicability of the Zimm theory for the polymer dynamics requires Sc to be much larger than one. For instance, in a real liquid like water $\mathrm{Sc}\approx 1000$. This condition implies that mass diffusion is much slower than momentum diffusion, and this is crucial for the validity of the Oseen tensor approximation. In the present work, the Schmidt number evaluated by the input kinematic viscosity and the numerically estimated fluid particle diffusivity is, as in DPD, of order 1. Nevertheless, scaling relations for the polymer dynamics have been recovered in good agreement with the Zimm theory with full hydrodynamic interactions. These results confirm the fact, already suggested by some authors [18,58], that the Schmidt number is an ill-defined quantity for coarse-graining models. There is therefore no need in principle to increase Sc but numbers of $O(1)$ can still produce the correct hydrodynamic behavior and, at the same time, provide a reasonable choice in terms of CPU time. In order to increase the artificial Schmidt number, a way would be to increase the kinematic viscosity with a numerical bottleneck due to the viscous time step limitation as a consequence. Realistic conditions could, however, be reached by using implicit schemes like those presented in [59,60], which are currently under investigation.

[1] G. E. Karniadakis and A. Beskok, *Micro Flows, Fundamentals and Simulations* (Springer, New York, 2002).

[2] S. C. Glotzer and W. Paul, Annu. Rev. Mater. Res. **32**, 401 (2002).

[3] A. Uhlherr and D. N. Theodorou, Curr. Opin. Solid State Mater. Sci. **3**, 544 (1998).

[4] H. A. Stone and S. Kim, AIChE J. **47**, 1250 (2001).

[5] M. Mertig, L. Colombi, R. Seidel, W. Pompe, and A. De Vita, Nano Lett. **2**, 841 (2002).

[6] S. Diez, C. Reuther, C. Dinu, R. Seidel, M. Mertig, W. Pompe, and J. Howard, Nano Lett. **3**, 1251 (2003).

[7] M. Mertig, L. Colombi, A. Benke, A. Huhle, J. Opitz, R. Seidel, H. K. Schackert, and W. Pompe, in *Foundations of Nanoscience: Self-Assembled Architectures and Devices*, edited by J. Reif (Science Technica, Snowbird, Utah, 2004), p. 132.

[8] L. D. Landau and E. M. Lifschitz, *Fluid Mechanics* (Pergamon Press, New York, 1959).

[9] B. Dünweg and K. Kremer, J. Chem. Phys. **99**, 6983 (1993).

[10] C. Aust, M. Kröger, and S. Hess, Macromolecules **32**, 5660 (1999).

[11] J. M. Polson and J. P. Gallant, J. Chem. Phys. **124**, 184905 (2006).

[12] R. Jendrejack, D. C. Schwartz, M. D. Graham, and J. J. de Pablo, J. Chem. Phys. **119**, 1165 (2003).

[13] K. Mussawisade, M. Ripoll, R. G. Winkler, and G. Gomper, J. Chem. Phys. **123**, 144905 (2005).

[14] P. Ahlrichs and B. Dünweg, J. Chem. Phys. **111**, 8225 (1999).

[15] P. J. Hoogerbrugge and J. Koelman, Europhys. Lett. **19**, 155 (1992).

[16] P. Español and P. Warren, Europhys. Lett. **30**, 191 (1995).

[17] N. A. Spenley, Europhys. Lett. **49**, 534 (2000).

[18] W. Jiang, J. Huang, Y. Wang, and M. Laradji, J. Chem. Phys. **126**, 044901 (2007).

[19] V. Symeonidis, G. E. Karniadakis, and B. Caswell, Phys. Rev. Lett. **95**, 076001 (2005).

[20] Y. Kong, C. W. Manke, W. G. Madden, and A. G. Schlijper, Tribol. Lett. **3**, 133 (1997).

[21] S. Chen, N. Phan-Thien, X.-J. Fan, and B. C. Khoo, J. Non-Newtonian Fluid Mech. **118**, 65 (2004).

[22] X. Fan, N. Phan-Thien, and S. Chen, Phys. Fluids **18**, 063102 (2006).

[23] X. Fan, N. Phan-Thien, and T. Ng, Phys. Fluids **15**, 11 (2003).

[24] The use of soft two-body potentials in DPD may allow for chain crossing (violating topological constraints [18]) as well as particle penetration to the walls in problems involving confined situations.

[25] P. Español and M. Revenga, Phys. Rev. E **67**, 026705 (2003).

[26] J. J. Monaghan, Annu. Rev. Astron. Astrophys. **30**, 543 (1992).

[27] R. A. Gingold and J. J. Monaghan, Mon. Not. R. Astron. Soc. **181**, 375 (1977).

[28] L. B. Lucy, Astron. J. **82**, 1013 (1977).

[29] J. M. Vianney and A. Koelman, Phys. Rev. Lett. **64**, 1915 (1990).

[30] B. Maier and J. O. Rädler, Phys. Rev. Lett. **82**, 1911 (1999).

[31] R. Azuma and H. Takayama, J. Chem. Phys. **111**, 8666 (1999).

[32] S. R. Shannon and T. C. Choy, Phys. Rev. Lett. **79**, 1455 (1997).

[33] E. Falck, O. Punkkinen, I. Vattulainen, and T. Ala-Nissila, Phys. Rev. E **68**, 050102(R) (2003).

[34] O. Punkkinen, E. Falck, I. Vattulainen, and T. Ala-Nissila, J. Chem. Phys. **122**, 094904 (2005).

[35] A. Milchev and K. Binder, J. Phys. II **6**, 21 (1996).

[36] Y. Kong, C. W. Manke, W. G. Madden, and A. G. Schlijper, Int. J. Thermophys. **15**(6), 1093 (1994).

[37] P. G. de Gennes, *Scaling Concepts in Polymer Physics* (Cornell University Press, Ithaca, NY, 1979).

[38] J. P. Morris, P. J. Fox, and Y. Zhu, J. Comput. Phys. **136**, 214 (1997).

[39] J. P. Morris, Int. J. Numer. Methods Fluids **33**, 333 (2000).

[40] X. Y. Hu and N. A. Adams, J. Comput. Phys. **213**, 844 (2006).

[41] Note that, unlike DPD, SDPD repulsive interparticle forces have a multibody character due to the dependency of the pressure term $P_i$ on the local value of the particle density $\rho_i = \Sigma_j m_j W_{ij}$. This is a remarkable property of the method which prevents particle crossing for monomers and confining walls.

[42] E. G. Flekkøy, P. V. Coveney, and G. de Fabritiis, Phys. Rev. E **62**, 2140 (2000).

[43] J. Bonet and T.-S. L. Lok, Comput. Methods Appl. Mech. Eng. **180**, 97 (1999).

[44] M. Ellero, P. Español, and E. G. Flekkøy, Phys. Rev. E **68**, 041504 (2003).

[45] M. Grmela and H. C. Öttinger, Phys. Rev. E **56**, 6620 (1997).

[46] H. C. Öttinger and M. Grmela, Phys. Rev. E **56**, 6633 (1997).

[47] P. Español, M. Serrano, and H. C. Öttinger, Phys. Rev. Lett. **83**, 4542 (1999).

[48] P. W. Randles and L. D. Libersky, Mech. Eng. **139**, 375 (1996).

[49] H. Takeda, S. M. Miyama, and M. Sekiya, Prog. Theor. Phys. **92**, 939 (1994).

[50] M. Ellero, M. Kröger, and S. Hess, Multiscale Model. Simul. **5**, 759 (2006).

[51] P. Español (private communication).

[52] Notice that the FENE polymer molecule introduces an additional length in the model. The contour length is an appropriate parameter to estimate this molecular size. According to [23], if $L_c$ denotes one segment of the molecular chain, its average value is of the order of $\sqrt{R_0^2/(b+5)}$, where $b=KR_0^2/(k_BT)$ is a dimensionless parameter approximately equal to 95 in our simulations. This gives $L_c \simeq 6.6\times 10^{-2}$ $\mu$m. The polymer contour length will be therefore $L=NL_c$ and assumes values ranging from $\simeq 1.3$ $\mu$m ($N=20$) to $\simeq 7$ $\mu$m ($N=100$) consistent with the contour lengths of λ-DNA molecules.

[53] M. Ellero, M. Kröger, and S. Hess, J. Non-Newtonian Fluid Mech. **105**, 35 (2002).

[54] M. Ellero and R. I. Tanner, J. Non-Newtonian Fluid Mech. **132**, 61 (2005).

[55] M. Doi and S. F. Edwards, *The Theory of Polymer Dynamics* (Clarendon, Oxford, 1986).

[56] P. Cifra and T. Bleha, Macromol. Theory Simul. **8**, 603 (1999).

[57] R. Jendrejack, D. C. Schwartz, M. D. Graham, and J. J. de Pablo, J. Chem. Phys. **120**, 2513 (2004).

[58] E. A. J. F. Peters, Europhys. Lett. **66**, 311 (2004).

[59] S. C. Whitehouse, M. R. Bate, and J. J. Monaghan, Mon. Not. R. Astron. Soc. **364**, 1367 (2005).

[60] T. Shardlow, SIAM J. Sci. Comput. **24**, 1267 (2003).